

# Learning quantum tomography from incomplete measurements

Mateusz Krawczyk,<sup>1</sup> Pavel Baláž,<sup>2</sup> Katarzyna Roszak,<sup>2</sup> and Jarosław Pawłowski<sup>1</sup>

<sup>1</sup>*Institute of Theoretical Physics, Wrocław University of Science and Technology,  
Wybrzeże Wyspiańskiego 27, 50-370 Wrocław, Poland*

<sup>2</sup>*FZU - Institute of Physics of the Czech Academy of Sciences,  
Na Slovance 1999/2, 182 00 Prague, Czech Republic*

We revisit quantum tomography in an informationally incomplete scenario and propose improved state reconstruction methods using deep neural networks. In the first approach, the trained network predicts an optimal linear or quadratic reconstructor with coefficients depending only on the collection of (already taken) measurement operators. This effectively refines the undercomplete tomographic reconstructor based on pseudoinverse operation. The second, based on an LSTM recurrent network performs state reconstruction sequentially, thus is scalable. It can also optimize the measurement sequence, which suggests a no-free-lunch theorem for tomography: by narrowing the state space, we gain the possibility of more efficient tomography by learning the optimal sequence of measurements. Numerical experiments for a 2-qubit system show that both methods outperform standard maximum likelihood estimation and also scale to larger 3-qubit systems. Our results demonstrate that neural networks can effectively learn the underlying geometry of multi-qubit states using this for their reconstruction.

## INTRODUCTION

Quantum state tomography (QST) [1–3] aims to determine the full state of a quantum system via a series of quantum measurements. Although the methods for complete state reconstruction are well known [2, 4], QST for incomplete data does not have a simple straightforward solution as the positivity criterion imposed on the state estimators makes analytical studies of such problems extremely difficult [5]. Approximate statistical-based methods for QST with an undercomplete or noisy measurement set are the maximum entropy (MaxEnt) principle [5–7], maximum likelihood estimation (MLE) [5, 7–9], or least-squares inversion [10].

Although QST scales exponentially in the system size, approximate methods that scale much better (polynomially) already appear using either the singular value thresholding method [11], or neural networks (NNs) [12]. On the other hand, classical shadow tomography [13, 14] utilizes the fact that predicting important properties of a many-body state (without necessarily fully characterizing the quantum state) requires only a polynomially-growing number of measurements [15]. Restricted Boltzmann machine (RBM) [16, 17], multilayer perceptron (MLP) [18, 19], convolutional NN [20], recurrent NN [12, 21], or conditional generative adversarial NN (CGAN) [22] fed by subsequent measurement snapshots that form an *informationally complete* system can be used to reconstruct certain classes of states, but most models (beside that of Ref. [21], or Ref. [23], but using integer programming) are not optimizing the sequence of measurements. NN-aided tomography can also converge much faster [19, 22] than other QST techniques, while attention-based NNs can be used to effectively denoise measurement data during QST [24]. Deep NNs have also shown their usability in recognizing quantum entangle-

ment [25–29], or discord [30].

In this work we focus on a different scenario; we examine various approaches to QST of general mixed states for *undercomplete* measurement data, but assuming that a single measurement outcome is known exactly, and show that NNs outperform standard estimators such as MLE on a diverse set ( $S_{\text{test}}$ ) of 2- and 3-qubit random mixed states. We explicitly demonstrate that neural estimators yield optimal reconstruction for the 1-qubit case and identify the best measurement sequence for 2-qubit X states.

## QUANTUM TOMOGRAPHY

In general, the outcome of a projection-valued measurement (PVM) can be written as [31]  $m = \mathcal{N} \text{Tr}(\hat{\mu} \hat{\rho})$ , where  $\hat{\mu}$  is the projection operator,  $\hat{\rho}$  is the density matrix, and  $\mathcal{N}$  is a constant of proportionality which can be determined from the data. For  $N$  qubits, the outcomes of joint measurements required for QST ( $4^N - 1$  outcomes in total) can be expressed as

$$m_{i_1, \dots, i_N} = \mathcal{N} \text{Tr}((\mu_{i_1} \otimes \dots \otimes \mu_{i_N}) \rho) = \mathcal{N} \text{Tr}(\Pi_{i_1, \dots, i_N} \rho), \quad (1)$$

where  $\mu_{i_k} = |i_k\rangle\langle i_k|$  are single-qubit projectors acting on the  $k$ -th qubit state. Then  $m_{i_1, \dots, i_N}$  estimates the probability that the system before a measurement was in a state represented by  $\Pi_{i_1, \dots, i_N} = \bigotimes_{k=1}^N \mu_{i_k}$ . In the following, we will use the standard set of measurement basis proposed by James et al. [2], where  $\mu_{i_k}$  are projections on the following states:

$$|i_k\rangle \in \{|0\rangle, |1\rangle, \frac{1}{\sqrt{2}}(|0\rangle + |1\rangle), \frac{1}{\sqrt{2}}(|0\rangle - |1\rangle)\}. \quad (2)$$

The operators meet the following conditions:  $\Pi_{i_1, \dots, i_N}$  are Hermitian, idempotent, and positive semidefinite. How-

ever, they do not sum to identity:  $\sum_{i_k=0}^3 \mu_{i_k} \neq \mathbf{1}_2$ , therefore  $\sum_{i_1, \dots, i_N=0}^3 \Pi_{i_1, \dots, i_N} \neq \mathbf{1}_{2^N}$ . They are also not trace-orthonormal,  $\text{Tr}(\mu_{i_k} \mu_{j_k}) \neq \delta_{ij}$ , and thus do not form PVM system [32]. Note that the completeness of PVM is not the same as the completeness of QST itself. Nevertheless, since the eigenvalues of the Gramian matrix  $\mathcal{G} = \text{Tr}(\Pi_{i_1, \dots, i_N} \Pi_{j_1, \dots, j_N}) = \bigotimes_{k=1}^N \text{Tr}(\mu_{i_k} \mu_{j_k}) = \text{Tr}(\mu_i \mu_j)^{\otimes N}$  are all positive, because  $\text{Det}(\mathcal{G}) = \text{Det}(\text{Tr}(\mu_i \mu_j))^{N 4^{N-1}} = (\frac{1}{4})^{N 4^{N-1}} \neq 0$  in our case, operators  $\Pi_{i_1, \dots, i_N}$  form a linearly independent set of dimension  $4^N$  and give a complete measurement basis [5].

To obtain a single outcome  $m_{i_1, \dots, i_N}$ , a set of  $N_c$ , typically thousands, projective measurements have to be performed, then  $m$  is estimated as  $n_c/N_c$ , where  $n_c$  is a number of coincidence counts in a measurement setup. Generally the state of an  $N$ -qubit system requires  $4^N - 1$  (due to trace-normalization) different measurement sets, each requiring  $N_c$  copies of the system.

After collecting a system of measurement outcomes  $m_{i_1, \dots, i_N}$  one can topographically reconstruct the state via the  $\Gamma_\mu$ -matrix basis [2]:

$$\rho = \Gamma_\mu (\langle \psi_\nu | \Gamma_\mu | \psi_\nu \rangle)^{-1}_{\mu\nu} m_\nu, \quad (3)$$

where the index  $\nu \equiv i_1, \dots, i_N$  collects indices of subsequent single-qubit operators, the tomographic state  $|\psi_\nu\rangle = |i_1\rangle \otimes \dots \otimes |i_N\rangle$  is composed of states defining subsequent projectors, and  $\Gamma_\mu = \bigotimes_{k=1}^N \sigma_{j_k}$  is the Kronecker product composed out of the Pauli matrices  $\sigma_{j_k}$ , with  $\mu \equiv j_1, \dots, j_N$  and  $j_k$  indexing the Pauli matrix of qubit  $k$ . The matrix  $B_{\nu\mu} = \langle \psi_\nu | \Gamma_\mu | \psi_\nu \rangle$  relates subsequent measurements  $m_\nu$  with the state representation in the  $\Gamma_\mu$  basis. The choice of measurement basis ( $\mu_{i_k} = |i_k\rangle\langle i_k|$ ) required to obtain full information about a quantum state  $\rho$  is not unique, but  $B_{\nu\mu}$  must be invertible.  $B_{\nu\mu} = \text{Tr}((\bigotimes_{k=1}^N \mu_{i_k})(\bigotimes_{k=1}^N \sigma_{j_k})) = \bigotimes_{k=1}^N \text{Tr}(\mu_{i_k} \sigma_{j_k}) = \text{Tr}(\mu_i \sigma_j)^{\otimes N}$ , and  $\text{Det}(B_{\nu\mu}) = \text{Det}(\text{Tr}(\mu_i \sigma_j))^{N 4^{N-1}}$  is nonzero because  $\text{Det}(\text{Tr}(\mu_i \sigma_j)) = -2 \neq 0$  in our case, so the condition is met.

### Incomplete measurement set

QST is extremely resource-intensive, so it is natural to ask what happens if we do not have a complete set of measurements or if we have measurements with a significant uncertainty. Here we will deal with the former case, that is, the number  $M$  of measurement operators ( $\Pi_\nu = |\psi_\nu\rangle\langle\psi_\nu|$ ) or outcomes ( $m_\nu$ ) is less than  $4^N - 1$  and they form an incomplete information set [5].

If the number of measurement operators  $M$  is smaller than the dimension of the complete set spanned by the  $4^N$   $\Gamma_\mu$  matrices in the linear QST,  $B_{\nu\mu}$  with dimension  $M \times 4^N$  is no longer a square matrix, and becomes noninvertible. The most natural way to keep the formula of Eq. (3) operational is to use the pseudoinverse

(Moore–Penrose inverse) [33] operation:  $(.)^+$ . Since measurement outcomes are linearly independent, so will the rows of matrix  $B_{\nu\mu}$  be, hence the formula for pseudoinverse:  $B_{\mu\nu}^+ = B_{\mu\nu}^\dagger (B_{\nu\mu} B_{\mu\nu}^\dagger)^{-1}$ . Then the reconstruction formula is

$$\rho \simeq \Gamma_\mu B_{\mu\nu}^+ m_\nu. \quad (4)$$

Using the pseudoinverse as a QST estimator was also discussed in Ref. [19]. In the results section we show that pseudoinverse-based reconstruction does not give the best possible solution, therefore, we try to construct better reconstruction schemes based on NN regressors.

### CORRECTOR NETWORK

In first attempt, we train a NN just to correct the pseudoinverse  $B_{\mu\nu}^+$  matrix by adding some correction term  $b_{\mu\nu}^{\text{NN}}$  in order to get the smallest possible reconstruction error averaged over the training set:

$$\rho_{\text{corr}}^{\text{NN}}(\mathcal{M}) = \Gamma_\mu ((B_{\mu\nu}^+ + b_{\mu\nu}^{\text{NN}}(\mathcal{M})) m_\nu + c_\mu^{\text{NN}}(\mathcal{M})), \quad (5)$$

where  $\mathcal{M} = \{(\Pi_\nu)_{\nu=1}^M, (m_\nu)_{\nu=1}^M\}$  is a collection of  $M$  different measurement operators and their outcomes, i.e. information obtained from measurements, determining the NN's input. The *corrector* NN has two outputs:  $\text{NN}_{\text{corr}}(\mathcal{M}) = (b_{\mu\nu}^{\text{NN}}(\mathcal{M}), c_\mu^{\text{NN}}(\mathcal{M}))$ . The second output,  $c_\mu^{\text{NN}}$  vector, is conceived to enable the model to predict normalized  $\rho^{\text{NN}}$ , irrespectively of the outcome values  $(m_\nu)_{\nu=1}^M$ ,  $M < 4^N$  (which no longer form a complete tomographic set). Moreover, if we take Eq. (5) and calculate element  $\langle \psi_{\nu'} | \cdot | \psi_\nu \rangle$  of both sides, we arrive at  $B_{\nu'\mu} \cdot v_\mu = 0$ ,  $v_\mu = b_{\mu\nu}^{\text{NN}} m_\nu + c_\mu^{\text{NN}}$  for all  $\nu' = 1..M$ , which means that the two NN outputs are not independent, and vector  $v_\mu$  must belong to the orthogonal complement of the subspace spanned by rows of  $B_{\nu'\mu}$ . To fulfill this condition, we added an extra component to the corrector NN loss during its training. Although the orthogonality condition speeds up training, it is not necessary: if we remove it, the corrector NN learns it anyway. It turns out that in the 1-qubit case, i.e.,  $N = 1$ , taking an appropriate (depending on the measurement basis  $(\mu_\nu)_{\nu=1}^{M < 4}$ ) orthogonal vector  $v_\mu$  (from the orthogonal complement) and choosing its norm so that  $\text{Tr}(\rho^{\text{NN}}) = 1$  is equivalent to taking the best possible analytical formula for the reconstruction, as discussed in the Appendix. However, for two and more qubits the choice is not so obvious anymore. Also, for a single qubit, the optimal  $b_{\mu\nu}^{\text{NN}}$  and  $c_\mu^{\text{NN}}$  do not depend on the results of measurements  $m_\nu$  (we can simply remove this information from training, getting the same results), which is not the case for  $N > 1$ .

We also introduced a modified corrector version  $\bar{\rho}_{\text{corr}}^{\text{NN}}(\Pi)$  that predicts coefficients using only the information about measurement operators (that do not depend on measurement outcomes) – defined in the same way as

in Eq. (5) but now  $\text{NN}_{\text{corr}}(\Pi) = (b_{\mu\nu}^{\text{NN}}(\Pi), c_{\mu}^{\text{NN}}(\Pi))$ , where we abbreviated  $\Pi \equiv (\Pi_{\nu})_{\nu=1}^M$ . One can also imagine improved version of the *corrector* NN, i.e. one containing a quadratic term:

$$\bar{\rho}_{\text{M}^2\text{-corr}}^{\text{NN}}(\Pi) = \bar{\rho}_{\text{corr}}^{\text{NN}}(\Pi) + \Gamma_{\mu} S_{\mu\nu\nu'}^{\text{NN}}(\Pi) m_{\nu} m_{\nu'}, \quad (6)$$

with the network  $S_{\mu\nu\nu'}^{\text{NN}}(\Pi)$  architecture designed in a way that the output tensor  $S_{\mu\nu\nu'}$  is symmetric – invariant under any measurements ( $\nu$  and  $\nu'$ ) permutation.

Note that the input layer size in all NN correctors ( $\rho_{\text{corr}}^{\text{NN}}(\mathcal{M})$ ,  $\bar{\rho}_{\text{corr}}^{\text{NN}}(\Pi)$ ,  $\bar{\rho}_{\text{M}^2\text{-corr}}^{\text{NN}}(\mathcal{M})$ ) depends on  $M$ . Due to its universality [34, 35], as our baseline model we choose a 6-layer fully connected (FC) network (multilayer perceptron) with 64 units (neurons) in each hidden layer and ReLU activations. The input/output layers are then adapted to meet the size  $M$ . Given the collection  $\mathcal{M}$  of measurements of size  $M$  and the training set of random density matrices  $S_{\text{train}}$  the NNs were trained to minimize the supervised training loss function:

$$\mathcal{L}(\mathcal{M}, S_{\text{train}}) = \frac{1}{N_b} \sum_i \|\rho_i - \rho_i^{\text{NN}}(\mathcal{M})\|, \quad (7)$$

where the difference between the original  $\rho_i \in S_{\text{train}}$  and the reconstructed  $\rho^{\text{NN}}$  is calculated averaging over a batch of size  $N_b = 64$ , and  $\|\cdot\|$  denotes a standard  $L^2$  norm. The batch is a random fraction of  $S_{\text{train}}$  used in a single step of the training procedure (typically when training NN the stochastic gradient descent method [35] is used). Random-sampling methods used to generate  $S_{\text{train}}$  are described in the Appendix.

## MEASUREMENTS SELECTOR NETWORK

NNs may become useful not only for reconstructing density matrix from the reduced number of measurement outcomes, but also for selecting the most important measurements. The general idea is to use two separate networks presented in Fig. 1, where the first one,  $\text{LSTM}_S$ , chooses the order of the measurements, and the second,  $\text{LSTM}_R$ , exploits the information contained in the measurements to reconstruct the density matrix effectively. We employ a recurrent network to memorize information from previous measurement collections across successive tomography steps. We utilize a popular LSTM [36] architecture in the form of six (one) unidirectional layers with 128 hidden units in the cell forming  $\text{LSTM}_{R(S)}$  network. Both networks are fed sequentially, which improves scalability, as the input size remains independent of  $M$ .

Randomly selecting a reduced set of measurements is not the best possible approach. Having partial information about the system (i.e. few already performed measurements) may allow the model to predict the next most promising measurement operator, which gives the most valuable information about the system. Especially,

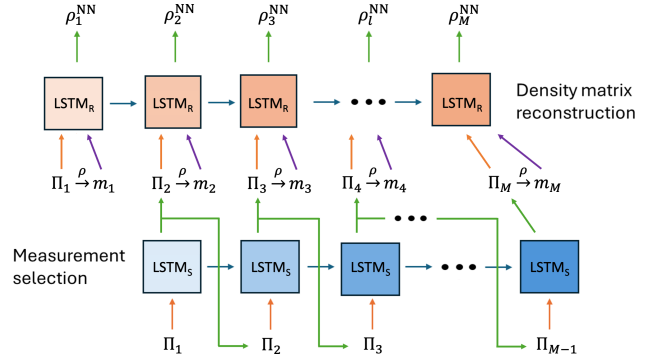


FIG. 1. Scheme for the neural-based measurements selection and reconstruction network. Having previous selection  $\Pi_{l-1}$ , the goal for the recurrent autoregressive  $\text{LSTM}_S$  unit is to propose the next measurement operator  $\Pi_l$ , which is used to measure the value  $m_l$ . Simultaneously, a pair  $(\Pi_l, m_l)$  is used as an input to  $\text{LSTM}_R$  cell, which outputs increasingly better reconstructions  $\rho_l$ , where  $l$  denotes the number of already performed measurements.

we propose to feed the  $\text{LSTM}_S$  with initial measurement basis  $\Pi_1 = \mu_0^{\otimes N}$  and force it to predict the next measurement operator  $\Pi_2$ , which is used to determinate value  $m_2$  according to Eq. (1). Subsequently, this procedure is repeated until the final choice  $\Pi_M$  is obtained.  $\text{LSTM}_S$  is a kind of *autoregressive* recurrent network with the output passed as the input in the next iteration.

Since there is no predetermined correct order of measurements, the typical approach of supervised training cannot be applied in this case. Instead, we combine the network responsible for measurement selection with the network performing the reconstruction,  $\text{LSTM}_R$ , as illustrated in Fig. 1. The selected measurement operators are passed along with the respective measurement values  $(\Pi_l, m_l)$  to the latter network, which at each step  $l$  aims to reconstruct the density matrix  $\rho_l^{\text{NN}}$ . To enable free information flow during *backpropagation* [35] (NN training), the measurement outcome algebra is incorporated directly into the NN architecture; however, during the test stage measurements can be provided externally. Finally, both networks are trained with the use of loss  $\mathcal{L}(S_{\text{train}}) = \frac{1}{N_b} \sum_{i,l} \|\rho_i - \rho_{i,l}^{\text{NN}}\|$ ,  $\rho_i \in S_{\text{train}}$  averaged over all selection-reconstruction steps  $l$ .

Two versions of the selector network  $\text{LSTM}_S$  were proposed and tested. The first approach at step  $l$  simply selects a previously unused measurement operator  $\Pi_l$  from the predefined basis  $\{\Pi_{i_1, \dots, i_N}\}$ , defined in Eq. (2). The second strategy is to allow  $\text{LSTM}_S$  to produce a *custom* measurement operator  $\Pi_l$ . The selected operator is then used to collect measurements and both the operator and the resulting measurements outcome are passed to the reconstruction network  $\text{LSTM}_R$ . One should also note that the first version needs discrete selections that typically utilize the *argmax* function, which is not differentiable. Therefore, to make the selection process dif-

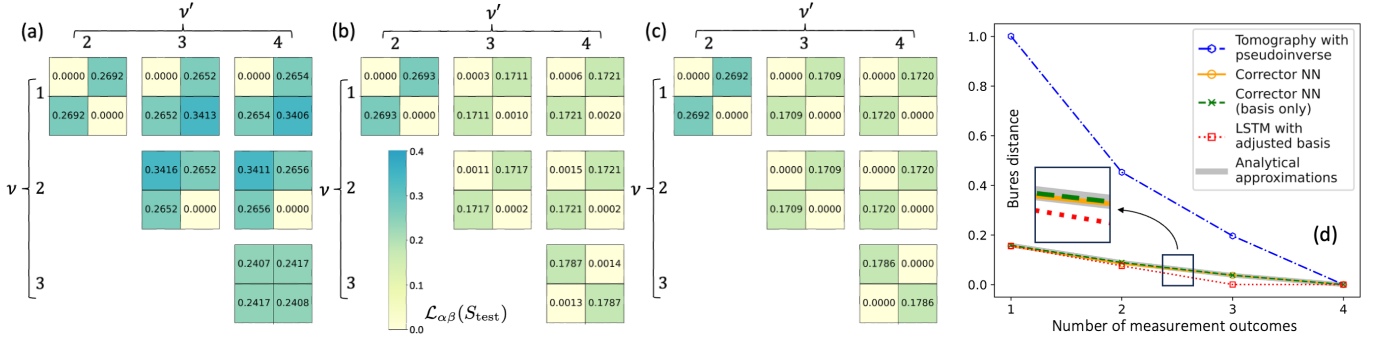


FIG. 2. Undercomplete 1-qubit density matrix tomography with two measurements  $(\nu, \nu')$ . (a-c) Element-wise reconstruction error  $\mathcal{L}_{\alpha\beta}(S_{\text{test}})$  using: (a) pseudoinverse reconstruction, (b) NN corrector, (c) best possible analytical formula. (d) Bures distance to target matrix averaged over  $S_{\text{test}}$  for the different techniques with increasing number of measurements.

ferentiable and thus enable backpropagation we applied the so-called *Gumbel-softmax* activation [37]. However, further experiments have shown that another approach with an additional loss term for the selector LSTM<sub>S</sub>, as discussed in the Appendix, worked better.

## RESULTS

In the next section, we demonstrate the effectiveness of the introduced NN-based QST through numerical experiments conducted on randomly generated single- and multi-qubit states. To describe the fidelity of a state reconstruction, we introduce a measure that quantifies the difference between ground-truth density matrix operators  $\rho$  and reconstructed ones  $\rho^{\text{NN}}$  using the so-called Bures distance [38, 39]:

$$\mathcal{B}(\rho^{\text{NN}}, \rho) = \sqrt{2 - 2\sqrt{F(\rho^{\text{NN}}, \rho)}}, \quad (8)$$

with the *fidelity*  $0 \leq F \leq 1$  defined as

$$F(\rho^{\text{NN}}, \rho) = \text{Tr} \left( \sqrt{\sqrt{\rho^{\text{NN}}} \rho \sqrt{\rho^{\text{NN}}}} \right)^2.$$

To collect prediction statistics, all of the examined NN correctors were trained using  $S_{\text{train}}$  for 100 measurement collections  $\mathcal{M}_j$  sampled without replacement (for the selector LSTM  $\mathcal{M}$  sampling is not needed). Then the average value of  $\langle \mathcal{B}(\rho_i^{\text{NN}}(\mathcal{M}_j), \rho_i) \rangle$  with  $\rho_i \in S_{\text{test}}$  was considered to validate the results. The whole procedure was repeated for  $M$  varying from 1 to  $4^N$ .

### 1-qubit system

As the first step of the evaluation, we verify the proposed approach for the trivial 1-qubit system. In Fig. 2 we present the reconstruction error for a 1-qubit density matrix, where we calculate the average error element-wise:  $\mathcal{L}_{\alpha\beta}(S_{\text{test}}) = \frac{1}{N_{\text{test}}} \sum_i \|\rho_{i,\alpha\beta} - \rho_{i,\alpha\beta}^{\text{NN}}\|$ ,  $\rho_i \in S_{\text{test}}$ .

We plot the results for different pairs of measurement operators  $(\nu, \nu')$ . One can notice that the NN corrector, as presented in Fig. 2(b), has almost the same structure of errors as the analytical formulas – Fig. 2(c), which give the best possible reconstruction for a given pair of measurements. These formulas can be easily found in a 1-qubit system and are discussed in the Appendix. What is characteristic, the optimal selection of  $b_{\mu\nu}^{\text{NN}}$  and  $c_{\mu}^{\text{NN}}$  does not depend on the measurement results  $m_{\nu}$  but only on the measurement operators  $\Pi_{\nu}$ . Therefore,  $\rho_{\text{corr}}^{\text{NN}}(\mathcal{M})$  (as well as  $\bar{\rho}_{\text{M}^2\text{-corr}}^{\text{NN}}(\mathcal{M})$ ) simply collapses to  $\bar{\rho}_{\text{corr}}^{\text{NN}}(\Pi)$ . Measurement outcomes  $m_{\nu}$  become relevant for the reconstruction of the 2-qubit and larger systems. It is worth noting that the optimal reconstruction found by NN outperforms an approximate one using the pseudoinverse – Fig. 2(a). The latter often has problems with preserving the trace-norm, as discussed in the Appendix.

Similar error precedence can be observed when examining the ( $S_{\text{test}}$ -averaged) reconstruction (error) measure  $\langle \mathcal{B} \rangle$ , for different numbers of measurements of a single qubit. Fig. 2(d) shows that the Bures distance for various QST techniques decreases with the number of measurements and approaches zero when  $M = 4$ . The reconstruction obtained with the NN corrector (orange curve) is much better than pseudoinverse (blue) and practically as good as the (best) analytical approximation (gray), which is discussed in the Appendix. The NN corrector that takes only information about the basis, i.e.  $(\Pi_{\nu})$ , (green) performs similarly. The LSTM model (red) additionally optimizes the measurement order, avoiding redundancy, and obtains a complete reconstruction just with  $M = 3$  measurements, that for 1-qubit setup with optimized choice of measurements (i.e. one that utilizes trace-normalization – see Appendix) are sufficient.

### 2-qubit system

Let us now move to a 2-qubit system, whose geometry is far more nontrivial [40–42] and even describing semi-

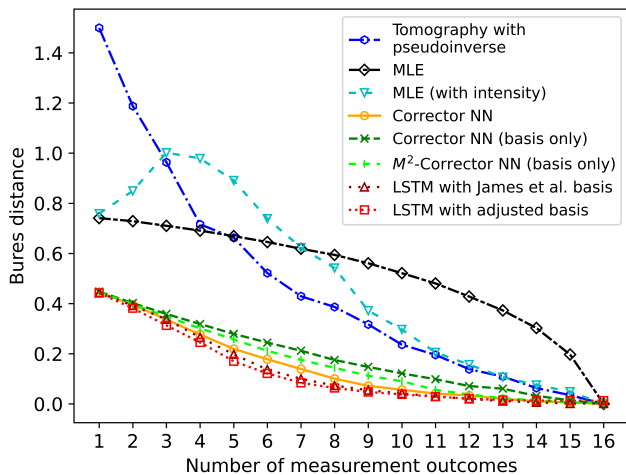


FIG. 3. Undercomplete 2-qubit tomography:  $S_{\text{test}}$ -averaged Bures distance to target matrix for the different reconstruction techniques with increasing number of measurements.

positivity is nontrivial itself. The average Bures distance  $\langle \mathcal{B} \rangle$  vs. the number of measurements  $M$  for different reconstruction approaches is presented in Fig. 3. Although all NN models achieve far better scores in density matrix reconstruction than the pseudoinverse-based QST (blue), they also outperform the MLE method-based reconstructions (computed using **Quantum-Tomography** library [43]) both when calculated with (light blue) and without (black) the *intensity* parameter. It informs the MLE which basis measurements were present (with intensity 1) or absent (with zero intensity) during the fitting process. When it comes to the NN corrector model, it is clear that including information about the measurement values in  $\rho_{\text{corr}}^{\text{NN}}(\mathcal{M})$  (orange), helps the NN to predict slightly more accurate corrections to the pseudoinverse method than  $\bar{\rho}_{\text{corr}}^{\text{NN}}(\Pi)$  (green). One can also observe that including the quadratic term in  $\bar{\rho}_{M^2\text{-corr}}^{\text{NN}}(\Pi)$  (light green), Eq. (6), gives better reconstruction than the linear model (green), but still worse than the measurement value-dependent one (orange), which suggests that the optimal reconstruction theory might include even higher-order measurement interactions.

Moreover, there is a visible improvement in performance for the LSTM recurrent networks, which are not only tasked with reconstructing (LSTM<sub>R</sub> network), but also to propose a sequence of measurement operators (LSTM<sub>S</sub>): the brown curve, in Fig. 3, presents Bures distance  $\langle \mathcal{B} \rangle$  for the model that selects measurement operators from a predefined basis, Eq. (2), while the red curve evaluates the model that proposes custom operators. The performance gain from adjusting the sequence  $(\Pi_\nu)$  suggests that some measurements are of greater importance in the  $S_{\text{train}}$  set, which we discuss further. An important observation is that the predefined basis selector (brown) collapses to a single measurement sequence

already during the training (albeit different trainings lead to different sequences); while the custom basis-selector (red) during tests follows various paths in the  $\Pi_l$  operator space, which proves that there are many equivalent possibilities for selecting optimal sequences of measurement bases.

## DISCUSSION

The above experiments show that it is possible to train an NN that is able to propose an optimal linear or quadratic reconstructor with constant coefficients depending only on the choice of the collection of measurement operators  $(\Pi_\nu)_{\nu=1}^M$ . For different sizes  $M$  of measurement collections (different sizes of the model input and output) we train separate corrector models.

To make the model independent of  $M$ , we also proposed another solution based on the LSTM recurrent network. This model sequentially selects consecutive measurements. In general, for an arbitrary state, there is no predefined optimal sequence of measurements, which are linearly independent operators. However, if we restrict the state space to a certain subclass, e.g. to so-called X states [44], certain sequences of measurements are preferable to others. By training the LSTM on X states, we obtained sequences like  $\nu = (1, 2, 6, 11, 16, 12, 15, \dots)$  or  $(1, 3, 14, 16, 12, 15, 11, \dots)$  (X state definition and measurements numbering is described in the Appendix). Typically, in the acquired sequences, the first three gave full information about the diagonal elements; while the next four (any permutation of  $(11, 12, 15, 16)$  measurements) gave full information about the coherences. This result shows that there is a tomographic equivalent of the *no free lunch* theorem [45, 46]: by restricting the state space, we gain the possibility of more efficient QST by learning the optimal (redundancy-free) sequence of measurements.

We also verified that both the corrector and the LSTM models reconstruct a positive semidefinite matrix: regardless of the measurement collection size  $M$ , the reconstructed matrix has the lowest eigenvalue that is on average always nonnegative (with a standard deviation  $\sim 0.01$  on  $S_{\text{test}}$ ). This proves that NNs have correctly learned the geometry of mixed states. We have also verified that the proposed NNs-based methods also scale up to 3-qubit systems, which we discuss in the Appendix.

## ACKNOWLEDGMENTS

MK and JP acknowledge support from National Science Centre, Poland, under grant no. 2021/43/D/ST3/01989. KR is funded within the QuantERA II Programme that has received funding from the EU H2020 research and innovation programme

under Grant Agreement No. 101017733, and with funding organization MEYS. This work was supported by the research programme of the Strategy AV21 AI: Artificial Intelligence for Science and Society. We gratefully acknowledge Polish high-performance computing infrastructure PLGrid (HPC Centers: ACK Cyfronet AGH) for providing computer facilities and support within computational grant no. PLG/2025/018433.

## APPENDIX

### Single-qubit tomography from incomplete measurement set: best approximation

Here we analyze the simplest single-qubit system ( $N = 1$ ) and show how the standard quantum tomography scheme extended via the pseudoinverse operation into incomplete measurements scenario, i.e.  $M = 2 < 4$ , behaves and in what way this behavior can be corrected.

Let us assume a density matrix in the following form:

$$\rho = \begin{pmatrix} a & b \\ b^* & 1-a \end{pmatrix}, \quad (\text{A1})$$

with real  $a \in [0, 1]$ , complex  $b$  with  $|b| \in [0, \frac{1}{2}]$  and  $a \geq a^2 + |b|^2$  to fulfill positive semidefiniteness condition. Then, the measurement outcomes (in the projector basis  $\Pi_\nu = \mu_{i_1} = |i_1\rangle\langle i_1|$ , with  $|i_1\rangle$  [defined in Eq. (2) in the main text] are  $(m_\nu)_{\nu=1}^4 = (a, 1-a, \frac{1}{2} + \text{Re}(b), \frac{1}{2} + \text{Im}(b))$ , thus  $B_{\nu\mu}$  matrix and its inverse are:

$$B_{\nu\mu} = \begin{pmatrix} 1 & 0 & 0 & 1 \\ 1 & 0 & 0 & -1 \\ 1 & 1 & 0 & 0 \\ 1 & 0 & -1 & 0 \end{pmatrix}, \quad B_{\mu\nu}^{-1} = \frac{1}{2} \begin{pmatrix} 1 & 1 & 0 & 0 \\ -1 & -1 & 2 & 0 \\ 1 & 1 & 0 & -2 \\ 1 & -1 & 0 & 0 \end{pmatrix}. \quad (\text{A2})$$

Finally, calculating  $\rho = \Gamma_\mu B_{\mu\nu}^{-1} m_\nu$  restores the original matrix  $\rho$  defined in Eq. (A1).

The situation changes if we reduce the number of projectors to two, e.g.,  $\nu = 1, 2$  by taking  $\mu_1, \mu_2$  with  $m_1 = a$  and  $m_2 = 1-a$  outcomes. Now  $B_{\nu\mu}$  [formed by two first rows of  $B_{\nu\mu}$  from Eq. (A2)] is no longer a square matrix and its inverse does not exist. However, one can calculate its pseudoinverse getting:

$$B_{\mu\nu}^+ = \frac{1}{2} \begin{pmatrix} 1 & 0 & 0 & 1 \\ 1 & 0 & 0 & -1 \end{pmatrix}^T, \quad (\text{A3})$$

and then reconstruct the state via  $\rho \simeq \Gamma_\mu B_{\mu\nu}^+ m_\nu$  (note that  $\nu = 1, 2$ ,  $\mu = 1, 2, 3, 4$ ) formula:

$$\rho_{\text{pseudoinv}} = \begin{pmatrix} a & 0 \\ 0 & 1-a \end{pmatrix}. \quad (\text{A4})$$

One can notice that the diagonal part of  $\rho_{\text{pseudoinv}}$  in Eq. (A4) is reconstructed correctly, while off-diagonal

terms are absent. The most important observation is that since  $m_1$  and  $m_2$  measurement outcomes contain only the information about populations, i.e.  $a$ , better reconstruction than Eq. (A4) is not possible and pseudoinverse scheme gives the best possible reconstruction and no corrections are needed.

However, when we select two other measurement outcomes:  $\nu = 1, 3$ , that is  $m_1 = a$  and  $m_3 = \frac{1}{2} + \text{Re}(b)$ , pseudoinverse will not give the best possible reconstruction. Now the pseudoinverse is

$$B_{\mu\nu}^+ = \frac{1}{3} \begin{pmatrix} 1 & -1 & 0 & 2 \\ 1 & 2 & 0 & -1 \end{pmatrix}^T, \quad (\text{A5})$$

leading to the reconstruction:

$$\rho_{\text{pseudoinv}} = \frac{1}{3} \begin{pmatrix} 3a & 1-a+2\text{Re}(b) \\ 1-a+2\text{Re}(b) & 1-a+2\text{Re}(b) \end{pmatrix}. \quad (\text{A6})$$

that is not even correctly normalized. Nevertheless, if we add the following correction terms:

$$b_{\mu\nu} = \frac{1}{3} \begin{pmatrix} -1 & 1 & 0 & 1 \\ -1 & 1 & 0 & 1 \end{pmatrix}^T, \quad c_\mu = \frac{1}{2} (1 \ -1 \ 0 \ -1)^T, \quad (\text{A7})$$

this via the formula  $\rho \simeq \Gamma_\mu ((B_{\mu\nu}^+ + b_{\mu\nu}) m_\nu + c_\mu)$  gives the best possible approximation:

$$\rho_{\text{corrected}} = \begin{pmatrix} a & \text{Re}(b) \\ \text{Re}(b) & 1-a \end{pmatrix}. \quad (\text{A8})$$

This shows that there is room for action for the NN *corrector* model compared to the scheme based on pseudoinverse. One can also verify that for terms defined in Eq. (A7) vector  $b_{\mu\nu} m_\nu + c_\mu = \frac{1-a-\text{Re}(b)}{3} (1, -1, 0, -1)^T$  is orthogonal to 1st and 3rd row in matrix  $B_{\nu\mu}$  from Eq. (A2). The same can be done for the other pairs of measurements obtaining various  $\rho_{\text{corrected}}$  for pairs of measurements  $(\nu, \nu')$

$$\nu \begin{matrix} \nu' \\ \left[ \begin{pmatrix} a & 0 \\ 0 & 1-a \end{pmatrix} \begin{pmatrix} a & \text{Re}(b) \\ \text{Re}(b) & 1-a \end{pmatrix} \begin{pmatrix} a & \text{Im}(b) \\ -\text{Im}(b) & 1-a \end{pmatrix} \right] \\ \begin{pmatrix} a & \text{Re}(b) \\ \text{Re}(b) & 1-a \end{pmatrix} \begin{pmatrix} a & \text{Im}(b) \\ -\text{Im}(b) & 1-a \end{pmatrix} \\ \begin{pmatrix} \frac{1}{2} & b \\ b^* & \frac{1}{2} \end{pmatrix} \end{matrix} \quad (\text{A9})$$

where rows denotes subsequent  $\nu = 1, 2, 3$  measurement outcome, while columns  $\nu' = 2, 3, 4$  outcome. The expressions in Eq. (A9) were used to generate the results shown in Fig. 2(c) of the main text.

### 2-qubit tomography: optimal ordering for $\mathbf{X}$ states.

The geometry of 2-qubit states is much more complicated than single-qubit ones [40–42]. To verify effectiveness of NN reconstruction in 2-qubit case we introduce a



family of so-called X states that generalize many important classes of mixed quantum states [44], but have much simpler structure than the general matrix:

$$X = \begin{pmatrix} a & 0 & 0 & w \\ 0 & b & z & 0 \\ 0 & z^* & c & 0 \\ w^* & 0 & 0 & d \end{pmatrix}, \quad (\text{A10})$$

with  $a + b + c + d = 1$ ,  $a, b, c, d \geq 0$ , and  $|z| \leq \sqrt{bc}$ ,  $|w| \leq \sqrt{ad}$ . Then the measurements in our basis,  $\Pi_\nu = \mu_{i_1} \otimes \mu_{i_2}$ , with  $\mu_{i_k} = |i_k\rangle\langle i_k|$  defined in Eq. (2) from the main text, are:

$$(m_\nu)_{\nu=1}^{16} = \begin{pmatrix} a, \\ b, \\ \frac{1}{2}(a+b), \\ \frac{1}{2}(a+b), \\ c, \\ d, \\ \frac{1}{2}(c+d), \\ \frac{1}{2}(c+d), \\ \frac{1}{2}(a+c), \\ \frac{1}{2}(b+d), \\ \frac{1}{4} + \frac{1}{2}(\text{Re}(w) + \text{Re}(z)), \\ \frac{1}{4} + \frac{1}{2}((\text{Im}(w) - \text{Im}(z))), \\ \frac{1}{2}(a+c), \\ \frac{1}{2}(b+d), \\ \frac{1}{4} + \frac{1}{2}((\text{Im}(w) + \text{Im}(z))), \\ \frac{1}{4} + \frac{1}{2}((\text{Re}(z) - \text{Re}(w))). \end{pmatrix} \quad (\text{A11})$$

Thus, some of the measurements are redundant, meaning that some orderings of measurements might be more optimal than others. This leaves room for the NN LSTM model to develop an optimization of the measurement sequence.

### Scaling up to 3-qubit system

Here we would just like to show that all presented methods can be scaled into larger systems – in this case to a 3-qubit system with  $4^3 = 64$  measurements as presented in Fig. A1. To maintain the similar reconstruction performance as for the 2-qubit case, we had to increase the

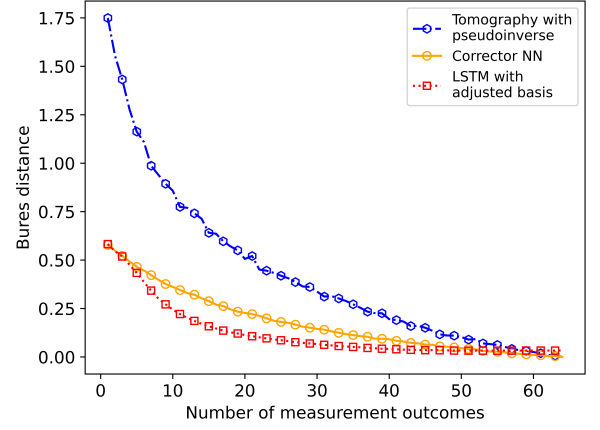


FIG. A1. Undercomplete 3-qubit tomography: average  $B$ -distance to target matrix for the different reconstruction techniques with increasing number of measurements.

number of hidden units in LSTM cells to 1024 (the number of layers remained unchanged: 6(1) for LSTM<sub>R(S)</sub>). In case of the corrector NN, the input layers have to be rescaled; however, we maintained the hidden network part the same as for the 2-qubit case (6 hidden FC layers with 64 units each). Increasing the number of hidden units to 1024 did not change the performance of the model. Nevertheless, determining the exact dependence of the models' scaling with the system size requires further studies.

By comparing the reconstruction performances in Figs. 2 and 3 of the main text with those in Fig. A1, we observe that as the number of qubits increases, the NN reconstructor converges faster. This might suggest that performance improves with system size. In reality, however, this apparent improvement is likely due to the fact that, as the state space grows, it becomes more difficult to uniformly cover the entire space through random sampling. Consequently, NN may learn specific features or biases present in the training data and exploit them for faster convergence.

### Additional loss in selector NN with predefined measurement basis

The issue with the first version of the LSTM (which selects measurement operators from the basis by James et al. [2]) is that the *argmax* function typically used in classifiers is not differentiable. Unfortunately, the Gumbel-softmax [37] activation function did not yield satisfactory results, therefore, we had to modify the architecture by extending the selector LSTM<sub>S</sub> loss. The second version of the LSTM network (with adjusted measurement operators) does not possess this drawback.

In our approach the selector network LSTM<sub>S</sub> at each step  $l$  predicts the probability vector  $P^l$  that contains

the probabilities  $p_{\nu_l}$  of choosing measurement operators  $\Pi_{\nu_l}$  from a predefined basis  $\{\Pi_{i_1, \dots, i_N}\} \equiv \{\Pi_{\nu}\}$ , given the previous pair  $(\Pi_{l-1}, m_{l-1})$ . For training purposes, in the given step  $l$  each possible measurement pair  $(\Pi_{\nu_l}, m_{\nu_l})$  is constructed and independently passed through the reconstruction network, resulting in set of  $\rho_{\nu_l}^{\text{NN}}$ , with  $\nu_l = 1, \dots, 4^N$ . Then,  $\mathcal{L}_{\nu_l}(S_{\text{train}}) = \frac{1}{N_b} \sum_i \|\rho_i - \rho_{i, \nu_l}^{\text{NN}}\|$ ,  $\rho_i \in S_{\text{train}}$  is calculated for each  $\nu_l$  to find  $\nu_l^*$  that minimizes the loss. Such  $\nu_l^*$  is then set as a target in the cross-entropy loss for the vector  $P^l$ :

$$\mathcal{L}_{\text{CE}}(P^l, \nu_l^*) = - \sum_{\nu_l} y_{\nu_l} \log(p_{\nu_l}), \quad (\text{A12})$$

where  $y_{\nu_l} = 1$  when  $\nu_l$  is equal to  $\nu_l^*$ , and  $y_{\nu_l} = 0$  otherwise. Finally, the  $\Pi_l$  is set as  $\Pi_{\nu_l = \text{argmax}(P^l)}$ , meaning that the measurement operator  $\Pi_l$  is chosen as the  $\Pi_{\nu_l}$  with the highest probability  $p_{\nu_l}$  in a given step  $l$ , but with additional restriction to preserve the uniqueness of measurements among all steps. Such  $\Pi_l$ , together with respective  $m_l$ , are subsequently used as input for the reconstruction network  $\text{LSTM}_R$  trained using the  $\mathcal{L}_l(S_{\text{train}})$ .

In contrast, in the second strategy, the  $\text{LSTM}_S$  network directly produce (a custom) measurement operator that can be passed to the reconstruction network and both models are simultaneously trained using the single loss  $\mathcal{L}(S_{\text{train}}) = \frac{1}{N_b} \sum_{i,l} \|\rho_i - \rho_{i,l}^{\text{NN}}\|$ ,  $\rho_i \in S_{\text{train}}$  averaged over all selection-reconstruction steps  $l$ . This approach allows for much faster training.

### Training dataset

We generate a set of density matrices by using different random-sampling methods. The main idea is to generate random states using the quantum circuits approach, but in order to have a well-diversified ensemble, we also use a technique based on sampling from the uniform Haar measure [47]. Additionally, to increase the number of maximally entangled states, we specifically include 20000 of them. All methods are described in detail in Ref. [25]. In total, we generate 460000 matrices for the training dataset  $S_{\text{train}}$  and 46000 matrices for the test set  $S_{\text{test}}$  for 2-qubit experiments. The sizes of the 3-qubit datasets were the same.

---

[1] K. Vogel and H. Risken, Determination of quasiprobability distributions in terms of probability distributions for the rotated quadrature phase, *Phys. Rev. A* **40**, 2847 (1989).  
[2] D. F. V. James, P. G. Kwiat, W. J. Munro, and A. G. White, Measurement of qubits, *Phys. Rev. A* **64**, 052312 (2001).  
[3] M. Paris and J. Rehacek, eds., *Quantum state estimation*, Lecture Notes in Physics, Vol. 649 (Springer Berlin Heidelberg, Berlin, Heidelberg, 2004).

[4] J. Altepeter, E. Jeffrey, and P. Kwiat, *Photonic state tomography* (Academic Press, 2005) pp. 105–159.  
[5] Y. S. Teo, J. Řeháček, and Z. Hradil, Informationally incomplete quantum tomography, *Quantum Measurements and Quantum Metrology* **1**, 57 (2013).  
[6] V. Bužek, 6 quantum tomography from incomplete data via maxent principle, in *Quantum State Estimation*, edited by M. Paris and J. Řeháček (Springer Berlin Heidelberg, Berlin, Heidelberg, 2004) pp. 189–234.  
[7] Y. S. Teo, H. Zhu, B.-G. Englert, J. Řeháček, and Z. Hradil, Quantum-state reconstruction by maximizing likelihood and entropy, *Phys. Rev. Lett.* **107**, 020404 (2011).  
[8] Z. Hradil, Quantum-state estimation, *Phys. Rev. A* **55**, R1561 (1997).  
[9] Z. Hradil and J. Řeháček, Efficiency of maximum-likelihood reconstruction of quantum states, *Fortschritte der Physik* **49**, 1083 (2001).  
[10] T. Opatrný, D.-G. Welsch, and W. Vogel, Least-squares inversion for density-matrix reconstruction, *Phys. Rev. A* **56**, 1788 (1997).  
[11] M. Cramer, M. B. Plenio, S. T. Flammia, R. Somma, D. Gross, S. D. Bartlett, O. Landon-Cardinal, D. Poulin, and Y.-K. Liu, Efficient quantum state tomography, *Nature Communications* **1**, 149 (2010).  
[12] J. Carrasquilla, G. Torlai, R. G. Melko, and L. Aolita, Reconstructing quantum states with generative models, *Nature Machine Intelligence* **1**, 155 (2019).  
[13] A. Acharya, S. Saha, and A. M. Sengupta, Shadow tomography based on informationally complete positive operator-valued measure, *Phys. Rev. A* **104**, 052418 (2021).  
[14] H.-Y. Huang, R. Kueng, and J. Preskill, Predicting many properties of a quantum system from very few measurements, *Nature Physics* **16**, 1050 (2020).  
[15] S. Aaronson, Shadow tomography of quantum states, *SIAM Journal on Computing* **49**, STOC18 (2020), <https://doi.org/10.1137/18M120275X>.  
[16] G. Torlai, G. Mazzola, J. Carrasquilla, M. Troyer, R. Melko, and G. Carleo, Neural-network quantum state tomography, *Nature Physics* **14**, 447 (2018).  
[17] A. Melkani, C. Gneiting, and F. Nori, Eigenstate extraction with neural-network tomography, *Phys. Rev. A* **102**, 022412 (2020).  
[18] T. Xin, S. Lu, N. Cao, G. Anikeeva, D. Lu, J. Li, G. Long, and B. Zeng, Local-measurement-based quantum state tomography via neural networks, *npj Quantum Information* **5**, 109 (2019).  
[19] D. Koutný, L. Motka, Z. c. v. Hradil, J. Řeháček, and L. L. Sánchez-Soto, Neural-network quantum state tomography, *Phys. Rev. A* **106**, 012409 (2022).  
[20] T. Schmale, M. Reh, and M. Gärttner, Efficient quantum state tomography with convolutional neural networks, *npj Quantum Information* **8**, 115 (2022).  
[21] Y. Quek, S. Fort, and H. K. Ng, Adaptive quantum state tomography with neural networks, *npj Quantum Information* **7**, 105 (2021).  
[22] S. Ahmed, C. Sánchez Muñoz, F. Nori, and A. F. Kockum, Quantum state tomography with conditional generative adversarial networks, *Phys. Rev. Lett.* **127**, 140502 (2021).  
[23] J. Li, S. Huang, Z. Luo, K. Li, D. Lu, and B. Zeng, Optimal design of measurement settings for quantum-state-tomography experiments, *Phys. Rev. A* **96**, 032307 (2017).



- (2017).
- [24] A. M. Palmieri, G. Müller-Rigat, A. K. Srivastava, M. Lewenstein, G. Rajchel-Mieldzióć, and M. Płodzień, Enhancing quantum state tomography via resource-efficient attention-based neural networks, *Phys. Rev. Res.* **6**, 033248 (2024).
  - [25] J. Pawłowski and M. Krawczyk, Identification of quantum entanglement with Siamese convolutional neural networks and semisupervised learning, *Phys. Rev. Appl.* **22**, 014068 (2024).
  - [26] N. Taghaddomi, A. Mani, A. Fahim, and A. Bakouei, Effective detection of quantum discord by using convolutional neural networks, *Quantum Machine Intelligence* **7**, 40 (2025).
  - [27] Y. Chen, Y. Pan, G. Zhang, and S. Cheng, Detecting quantum entanglement with unsupervised learning, *Quantum Science and Technology* **7**, 015005 (2021).
  - [28] N. Asif, U. Khalid, A. Khan, T. Q. Duong, and H. Shin, Entanglement detection with artificial neural networks, *Scientific Reports* **13**, 1562 (2023).
  - [29] J. Ureña, A. Sojo, J. Bermejo-Vega, and D. Manzano, Entanglement detection with classical deep neural networks, *Scientific Reports* **14**, 18109 (2024).
  - [30] M. Krawczyk, J. Pawłowski, M. M. Maśka, and K. Roszak, Data-driven criteria for quantum correlations, *Phys. Rev. A* **109**, 022405 (2024).
  - [31] M. A. Nielsen and I. L. Chuang, *Quantum Computation and Quantum Information: 10th Anniversary Edition* (Cambridge University Press, 2010).
  - [32] R. Yuan, A brief introduction to POVM measurement in quantum communications (2022), arXiv:2201.07968 [quant-ph].
  - [33] R. Penrose, A generalized inverse for matrices, *Mathematical Proceedings of the Cambridge Philosophical Society* **51**, 406–413 (1955).
  - [34] K. Hornik, M. Stinchcombe, and H. White, Multilayer feedforward networks are universal approximators, *Neural networks* **2**, 359 (1989).
  - [35] P. Grohs and G. Kutyniok, *Mathematical aspects of deep learning* (Cambridge University Press, 2023).
  - [36] Y. Yu, X. Si, C. Hu, and J. Zhang, A Review of Recurrent Neural Networks: LSTM Cells and Network Architectures, *Neural Computation* **31**, 1235 (2019), [https://direct.mit.edu/neco/article-pdf/31/7/1235/1053200/neco\\_a.01199.pdf](https://direct.mit.edu/neco/article-pdf/31/7/1235/1053200/neco_a.01199.pdf).
  - [37] E. Jang, S. Gu, and B. Poole, Categorical reparameterization with gumbel-softmax, arXiv preprint arXiv:1611.01144 (2016).
  - [38] I. Bengtsson and K. Życzkowski, *Geometry of Quantum States: An Introduction to Quantum Entanglement* (Cambridge University Press, Cambridge, 2006).
  - [39] A. Gilchrist, N. K. Langford, and M. A. Nielsen, Distance measures to compare real and ideal quantum processes, *Phys. Rev. A* **71**, 062310 (2005).
  - [40] O. Gamel, Entangled bloch spheres: Bloch matrix and two-qubit state space, *Phys. Rev. A* **93**, 062320 (2016).
  - [41] L. Jakóbczyk and M. Siennicki, Geometry of bloch vectors in two-qubit system, *Physics Letters A* **286**, 383 (2001).
  - [42] M. Kuś and K. Życzkowski, Geometry of entangled states, *Phys. Rev. A* **63**, 032307 (2001).
  - [43] S. Turro, **Quantum-Tomography**: A python library to help perform tomography on a quantum state, <https://quantumtomo.web.illinois.edu/> (2023), version 1.0.7.0.
  - [44] A. A.-Q. Nicolás Quesada and D. F. James, Quantum properties and dynamics of X states, *Journal of Modern Optics* **59**, 1322 (2012), <https://doi.org/10.1080/09500340.2012.713130>.
  - [45] D. H. Wolpert, The lack of a priori distinctions between learning algorithms, *Neural computation* **8**, 1341 (1996).
  - [46] D. Wolpert and W. Macready, No free lunch theorems for optimization, *IEEE Transactions on Evolutionary Computation* **1**, 67 (1997).
  - [47] F. Mezzadri, How to generate random matrices from the classical compact groups, *Notices of the American Mathematical Society* **54** (2006).